Predicting Electrocatalytic Properties: Modeling Structure–Activity Relationships of Nitroxyl Radicals

David P. Hickey,[†,∥] David A. Schiedler,[†,∥] Ivana Matanovic,[‡,§] Phuong Vy Doan,[†] Plamen Atanassov,[‡] Shelley D. Minteer,*,[†] and Matthew S. Sigman*,[†]

[†]Department of Chemistry, University of Utah, Salt Lake City, Utah 84112, United States
[‡]Department of Chemical & Biological Engineering, University of New Mexico, Albuquerque, New Mexico 87131, United States
[§]Theoretical Division, Los Alamos National Laboratory, Los Alamos, New Mexico 87545, United States

Ⓢ Supporting Information

ABSTRACT: Stable nitroxyl radical-containing compounds, such as 2,2,6,6-tetramethylpiperidine-N-oxyl (TEMPO) and its derivatives, are capable of electrocatalytically oxidizing a wide range of alcohols under mild and environmentally friendly conditions. Herein, we examine the structure–function relationships that determine the catalytic activity of a diverse range of water-soluble nitroxyl radical compounds. A strong correlation is described between the difference in the electrochemical oxidation potentials of a compound and its electrocatalytic activity. Additionally, we construct a simple computational model that is able to accurately predict the electrochemical potential and catalytic activity of a wide range of nitroxyl radical derivatives.
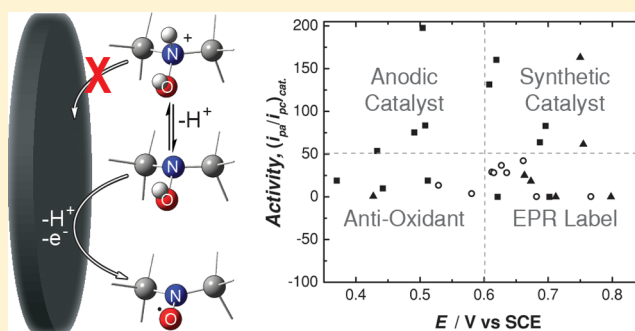
INTRODUCTION

Since their discovery in 1960, stable nitroxyl radicals have attracted tremendous attention due to their unique paramagnetic and redox characteristics.[1,2] The applications of these nitroxyl radical-containing compounds are diverse including their use as mechanistic tools for the detection of free radicals,[3−6] contrast agents for magnetic resonance imaging (MRI) in biological settings,[7−10] analytical tools for the detection of reactive oxygen species,[11−13] and, perhaps, most extensively as oxidative dehydrogenation catalysts.[3,14−23] In particular, readily available (2,2,6,6-tetramethylpiperidin-1-yl)-oxyl (TEMPO) has been exploited for its ability to electrocatalytically oxidize alcohols[24−27] and amines[28] under mild and environmentally benign reaction conditions. Despite the vast wealth of literature on TEMPO-mediated oxidations, there remain central mechanistic aspects and structure−activity relationships about this class of compounds that are not well understood.

Three electrochemically accessible oxidation states exist for TEMPO and its derivatives including a hydroxylamine (**TH**), a nitroxyl radical (**T***), or an oxoammonium cation (**T⁺**). During catalytic oxidation of an alcohol (as shown in Figure 1A), TEMPO is electrochemically oxidized from **T*** to the corresponding **T⁺**, which operates as the catalytically active species. An alcohol-containing substrate undergoes nucleophilic attack on the nitrogen of **T⁺** to form a TEMPO-substrate intermediate complex. A subsequent two-electron oxidation of the substrate yields the corresponding aldehyde and the

reduced **TH** species.[29,30] The active form of the catalyst is then electrochemically regenerated by an overall one proton coupled-two-electron oxidation of **TH**.[31] In aqueous conditions, the second oxidative step is presumed to be turnover limiting.[30] However, the exact nature of the oxidative regeneration of **T⁺** is not well understood.[32]

A wide range of hypotheses have been proposed to correlate the structure of TEMPO derivatives to their catalytic activity with >100 structural analogues synthesized and studied to date.[17,33−35] Many of the early reports suggest explanations for structure−activity relationships, which involve a predominantly steric argument with respect to the geminal dimethyl groups.[36] However, more recent efforts show a correlation of the **T***/**T⁺** oxidation potential with catalytic activity.[37,38] These proposed explanations are able to accurately account for defined subsets of TEMPO derivatives but fail to describe trends for broader classes of nitroxyl radical catalysts due in part to the examination of relatively small data sets.

A goal of our program is to utilize nitroxyl radical catalysts for a diverse range of electrocatalytic applications including fuel cells and batteries; therefore, the ability to predict the performance (oxidation potential and catalytic activity) of any nitroxyl radical catalyst would streamline our efforts. Additionally, understanding the mechanistic foundations associated with the structure function relationships would provide the
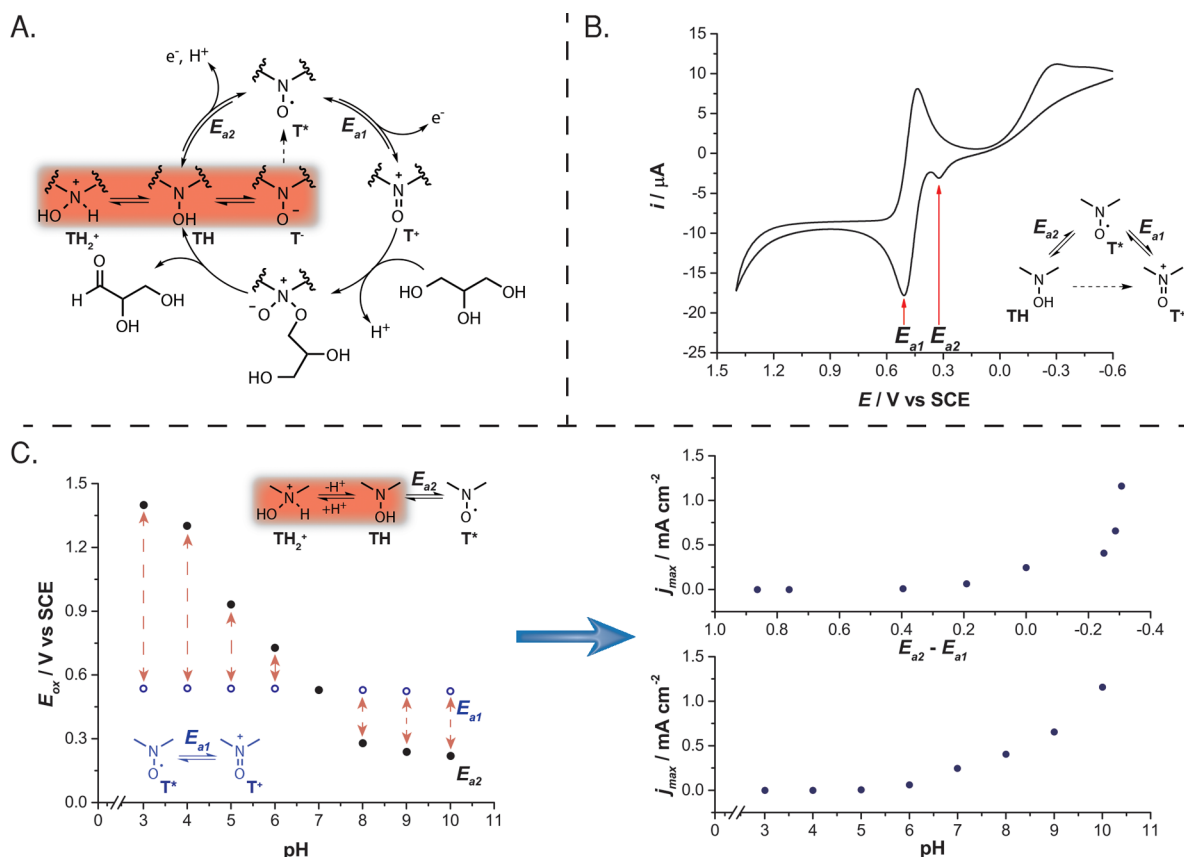
Figure 1. Presumed catalytic cycle for alcohol oxidation by TEMPO (A) that highlights the two external oxidation steps, E_{a1} and E_{a2}; a representative cyclic voltammogram of a nitroxyl radical (B) demonstrating how E_{a1} and E_{a2} are observed experimentally, and; the pH profile of catalytic activity (j_{max}) toward glycerol and oxidation potentials E_{a1} and E_{a2} for TEMPO (C). The pH profile of TEMPO indicates a correlation between the difference in E_{a1} and E_{a2} with the catalytic activity.

community a clearer picture of how to select an appropriate catalyst. Herein, we describe the synthesis, electrochemical characterization, and computational modeling of a range of nitroxyl radicals to reveal the salient features responsible for performance. These studies provide the basis to correlate and predict both the electrochemical potential and catalytic activity for new nitroxyl radical-based electrocatalysts under aqueous conditions.

■ **RESULTS AND DISCUSSION**

pH-Dependent Electrochemical Properties of TEMPO. We previously reported on the anomalous catalytic activity and expanded pH range of 4-amino-TEMPO.[39] It was observed that the reversible oxidation potential of amino-TEMPO is strongly pH dependent whereas the oxidation potential for unmodified TEMPO is independent of pH. This data compelled us to suggest that the uncharacteristic activity of amino-TEMPO must be related to its unique pH dependence, and consequently that TEMPO activity may be described as a function of redox potentials. To probe this hypothesis, we first examined the electrochemical characteristics and catalytic activity of TEMPO derivatives as a function of pH by using glycerol oxidation as a model reaction and unmodified TEMPO as an initial electrocatalyst.

As described above, the general mechanism for the electrocatalytic oxidation of alcohols by TEMPO is thought to proceed through two electrooxidative steps; the first occurs at an oxidation potential of E_{a1} corresponding to the oxidation

of **T*** to **T$^+$**, while the second occurs at an oxidation potential defined as E_{a2} corresponding to the proton-coupled oxidation of **TH** to **T***. A representative cyclic voltammogram (CV) shown in Figure 1B highlights the experimental determination of E_{a1} and E_{a2} for a nitroxyl radical species. The observed values for E_{a1} follow expected Nernst kinetics; however, values for E_{a2} were highly dependent on scan rate and frequently overlapped with the peaks for E_{a1}. Therefore, E_{a2} was determined experimentally using variable scan rates and extrapolating to a standard scan rate (a more complete discussion on the experimental determination of electrochemical parameters can be found in the Supporting Information Section S2.1).

The examination of both E_{a1} and E_{a2} of unmodified TEMPO as a function pH (shown in Figure 1C) indicates that, as mentioned above, E_{a1} is independent of proton concentration but that E_{a2} is inversely proportional to pH and thus dramatically decreased under basic conditions. This is due to the equilibrium that exists between the hydroxylamine form of TEMPO (**TH**) and its conjugate acid hydroxylammonium (**TH$_2^+$**).[40] Under acidic conditions, the **TH$_2^+$** form is favored and corresponds to an increased oxidation potential. In this manner, the pH profile of E_{a2} serves as a titration curve for the formation of **TH$_2^+$** and suggests a pK_a ≈ 5.5. This value is in good agreement with the reported literature pK_a for similar hydroxylamines.[41−43] Due to the uneven dependence of E_{a1} and E_{a2} on proton concentration, the equilibrium between **TH** and **TH$_2^+$** can be described in terms of the difference of the two
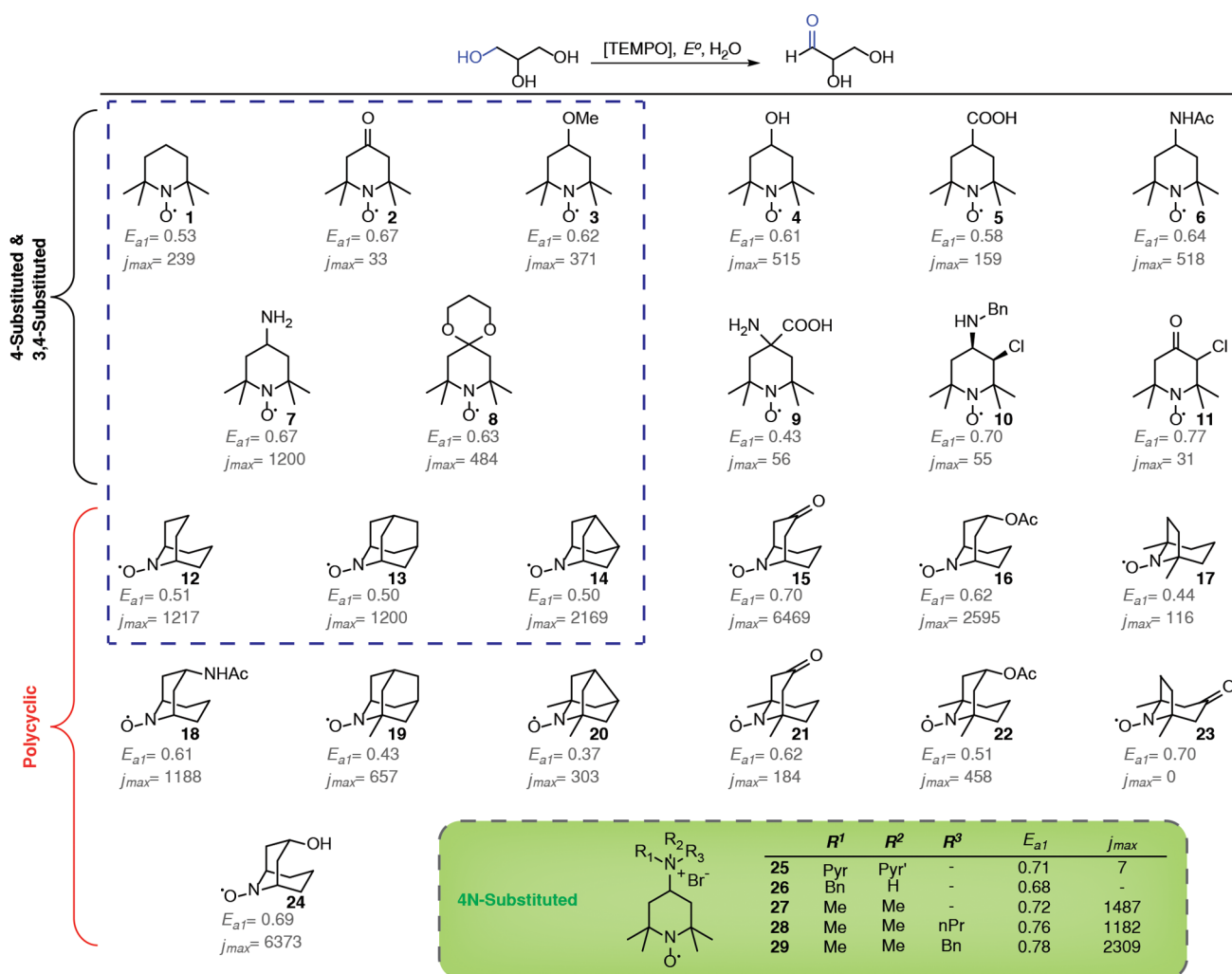
Figure 2. Summary of the nitroxyl radical catalysts screened for this study. A representative training set (indicated by the dashed enclosure, top left) was used to determine trends for both experimental and computational properties. All values for j_{max} were determined voltammetrically using a 200 mM Robinson buffer at pH 7.0 and 25 °C.

potentials. Therefore, as $E_{a2} - E_{a1}$ decreases and eventually becomes negative, the equilibrium shifts to favor **TH**.

In addition to E_{a2}, the electrocatalytic activity of TEMPO toward glycerol oxidation is also dependent on pH (as shown in Figure 1C), where the maximum catalytic current density (j_{max}) increases exponentially at higher pH. A similar trend can be drawn between $E_{a2} - E_{a1}$ and j_{max} in which the catalytic activity of TEMPO increases as E_{a2} decreases with respect to E_{a1}. The pH-dependence of TEMPO activity has been reported previously; however, the simultaneous correlation between j_{max}, pH, and $E_{a2} - E_{a1}$ indicates that the equilibrium between **TH** and **TH$_2^+$** is directly linked to the electrocatalytic activity of TEMPO. In other words, this correlation suggests that the catalytic activity of TEMPO is retarded by the formation of **TH$_2^+$** and the extent of this deactivation can be observed through the measurement of E_{a1} and E_{a2}.

Expansion of Potential−Activity Model. To test the validity of the hypothesis that j_{max} and $E_{a2} - E_{a1}$ are correlated, we synthesized (for synthetic procedures and characterization see the SI) and electrochemically evaluated a range of nitroxyl radical-containing compounds. The set included various functionalized TEMPO derivatives with different substitution patterns, bicyclic cores, and functional groups. While many of

these analogues have been previously prepared, the comprehensive electrochemistry in water has not been determined. A summary of the compounds with their reversible oxidation potential and absolute catalytic activity in the form of j_{max} are depicted in Figure 2. A significant range of electrochemical potential and catalytic activity is afforded with this group of electrocatalysts. The results qualitatively agree with the proposed hypothesis that destabilization of **TH$_2^+$** should result in higher activity. For example, amino-TEMPO (**7**), the initial inspiration for this study, possesses an ammonium cation under neutral aqueous conditions. This presumably disfavors the further protonation of its corresponding **TH** form. Consequently, **7** exhibits much higher activity than **5**, which possesses a carboxylate anion under the same conditions and can act to stabilize the resultant **TH$_2^+$** species. Consistent with these observations, the incorporation of a permanent ammonium cation in **29** results in the largest j_{max} for all monocyclic TEMPO derivatives.

Additionally, qualitative analysis of several commonly used polycyclic nitroxyl electrocatalysts such as derivatives of 9-azabicyclo[3.3.1]nonane N-oxyl (ABNO, **12**), 2-azaadamantane N-oxyl (AZADO, **13**), and 2-azanoradamantane N-oxyl (norAZADO, **14**) were studied with and without geminal

methyl groups relative to the nitroxyl nitrogen atom. A lower j_{max} for all geminal methyl-containing compounds is observed relative to the corresponding unmethylated derivative (compare **13** to **19**, **14** to **20**, **15** to **21**, and **16** to **22**). This trend can be explained by steric effects as others have alluded;[36] however, an alternate explanation can be offered through stabilization of **TH₂⁺**. The enhanced basicity of the methyl-containing structures stabilize **TH₂⁺** and accordingly result in a lower catalytic activity for these analogues.

It should be noted that some of the compounds in this study exhibited either autocatalytic behavior or comproportionation, which led to an artificially inflated j_{max} (the absolute j_{max} is reported in Figure 2). In order to test the quantitative correlation between catalytic activity and destabilization of **TH₂⁺** (via $E_{a2} - E_{a1}$), we used the ratio of the peak oxidative current, i_{pa}, and the peak reductive current, i_{pc}, to describe the normalized catalytic activity as $(i_{pa}/i_{pc})_{cat}$. A plot of $(i_{pa}/i_{pc})_{cat}$ versus ΔE_a (where $\Delta E_a = E_{a2} - E_{a1}$) for all nitroxyl radical species at pH 7 is shown in Figure 3A. An asymptotic relationship between electrocatalytic activity and ΔE_a for nitroxyl radical catalysts is observed where the catalytic activity approaches infinity as ΔE_a approaches −0.180 V. This correlation can be subsequently linearized by taking the inverse of the sum of ΔE_a plus the asymptotic limit. The resulting plot,

Figure 3. Plot indicating an asymptotic relationship between ΔE_a and $(i_{pa}/i_{pc})_{cat}$ for the nitroxyl radicals studied (A) and linearized plot (B) highlighting the 4-substituted (○) and 4N-substituted (▲) TEMPO derivatives, polycyclic species (■). The values shown in these plots were determined voltammetrically in 200 mM Robinson buffer at pH 7.0 and at 25 °C.

shown in Figure 3B, demonstrates an excellent linear correlation between $(i_{pa}/i_{pc})_{cat}$ and $(\Delta E_a+0.18)^{-1}$ with $R^2 = 0.92$.

The plots in Figure 3 indicate that there is a lower limit to the extent to which E_{a2} can be lowered with respect to E_{a1}. The precise source of this limit is not completely understood; however, the value of this limit (−0.180 eV = −4.15 kcal mol⁻¹) closely corresponds with the energy associated with hydrogen bond interactions between an aliphatic alcohol and a single water molecule.[44] This suggests that the source of the non-zero limit is a lowering of E_{a2} caused by hydrogen bonding assistance with the proton-coupled oxidation. Therefore, the catalytic activity is maximized when the thermodynamic potential for E_{a1} is equal to that of E_{a2}. This assertion is speculative and further studies are needed to conclusively determine the source of the observed limit. Nevertheless, the experimental correlation between activity and ΔE_a provides a means to predict catalytic activity as a function of two computationally accessible parameters, E_{a1} and E_{a2}.

Computational Prediction of Electrochemical Potential and Activity. Using the correlation described above, we developed a computational model to predict both the electrochemical potentials E_{a1} and E_{a2} and subsequently the catalytic activity for nitroxyl radical catalysts. A training set of TEMPO derivatives (highlighted in Figure 2) was used to derive trends in the computational modeling, and the remaining compounds were used to validate or refute the preliminary models. The training set was selected to represent the structural and electronic diversity of the nitroxyl radical species studied as well as a range of electrocatalytic activities observed.

Several reports have previously conveyed the computational prediction of E_{a1} from the solvated free energy cycle;[45,46] however, only a limited number of studies have been performed to demonstrate the prediction of E_{a2}.[47] In recent work by Hodgson et al., the irreversible one-electron reduction potentials (**T* → T⁻**) for several TEMPO derivatives were computationally predicted, but their report did not account for multiple protonation states of the reduced species (i.e., **TH₂⁺**, **TH**, **T⁻**).[47] Additionally, the experimentally determined Nernstian kinetics derived previously for the oxidation potentials associated with TEMPO derivatives do not take into consideration intramolecular protonation states (such as those associated with TEMPO-carboxylic acid, **5**, or amino-TEMPO, **7**). Therefore, we derived modified Nernstian kinetic equations to account for the possible protonation states, which were used for all computational modeling described herein. A more detailed discussion of these kinetic equations along with a complete derivation can be found in the Supporting Information.

Electrochemical potentials were determined using DFT calculations to compute the thermally corrected free energies for optimized structures of derivatives in each of their oxidation/protonation states (**TH₂⁺**, **TH**, **T***, **T⁺**). Free energies were calculated using Gaussian 09W with B3LYP/6-31+G(d,p) level of theory and basis set and CPCM continuum solvation model.[48,49] For E_{a1}, the free energy difference between **T⁺** and **T*** (ΔG_{a1}, in kJ mol⁻¹) was converted into an electrochemical potential and a correction factor was added to normalize the calculated potential to a saturated calomel reference electrode by

$$E_{a1} = -\frac{\Delta G_{a1}}{nF} - 4.68$$

Where n is the number of electrons transferred (for all oxidations described herein, $n = 1$), F is Faraday's constant ($F = 96.485$ kJ mol^{-1}) and 4.68 corresponds to the combined normalization factors to report E_{a1} relative to SCE.[50] A plot of predicted versus experimental values for E_{a1} (Figure 4A)
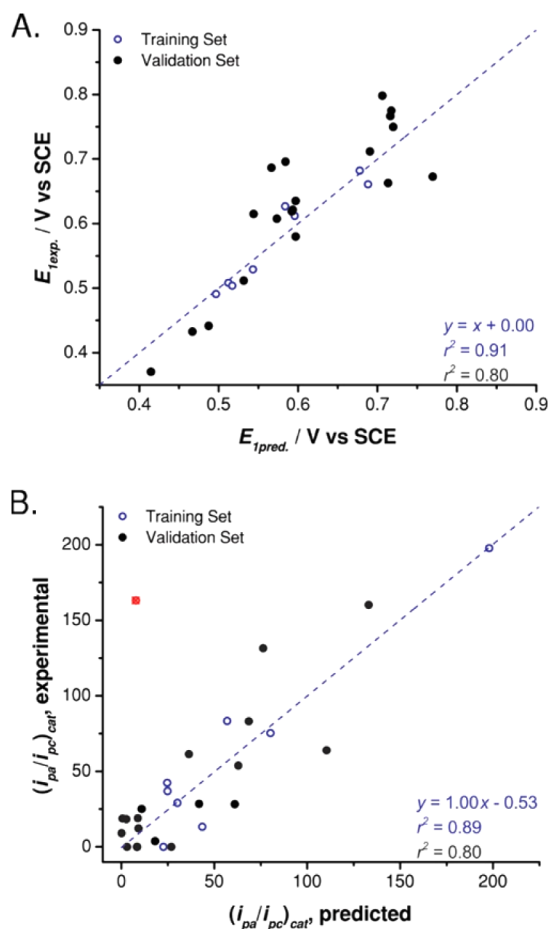
Figure 4. Plots of the computationally derived values of E_{a1} (A) and $(i_{pa}/i_{pc})_{cat}$ (B) versus their corresponding experimental values. Calculated r^2 values for the training set (blue) and validation set (black) are provided for each graph. Computations were performed using B3LYP/6-31+G(d,p) level of theory and basis set with a CPCM solvation model and assumed conditions of pH 7.0 and 25 °C as described in the Supporting Information.

demonstrates a good linear correlation between expected and observed values for the reversible oxidation potential between T^+ and T^* of the training set and validation set ($R^2 = 0.91$ and $R^2 = 0.80$ respectively). Additionally, the predicted trend provides an accurate prediction of the validation set. As mentioned above, values of E_{a2} were calculated similarly from the free energy cycle associated with the oxidation of TH to T^*. However, the calculation of E_{a2} from the free energy of the oxidation step required that various protonation steps be accounted for and that the Nernst equation be modified accordingly. Complete analysis of these computations and derivations of the modified reaction kinetics are provided in the Supporting Information.

The computationally predicted values of E_{a1} and E_{a2} were used to draw a correlation between $(\Delta E_{a,computational})^{-1}$ and the catalytic activity of the compounds in the training set. This trend was subsequently used as a model to predict the catalytic

activity for the validation set. The resulting plot of the predicted versus experimental values of $(i_{pa}/i_{pc})_{cat}$ (Figure 4B) demonstrates that both the training set and validation set provide a good linear correlation between predicted and observed activity ($R^2 = 0.89$ and $R^2 = 0.80$ respectively). A single deviation from the expected activity (shown as a red point in Figure 4B) is the result of a lack convergence for the TH_2^+ species of compound **29**. This is likely due to both the size of the catalyst and the presence of a permanent cation. Nevertheless, the model demonstrated here provides a convenient means of predicting both electrochemical potential and catalytic activity of nitroxyl radical oxidation catalysts under aqueous conditions.

Structure−Function Relationships from Computational Analysis. In addition to a quantitative model for predicting redox potential and catalytic activity of nitroxyl radicals demonstrated in the previous section, we sought to use DFT calculations to determine simple structure−function relationships that would provide a chemically intuitive model to aid in the rational design of novel TEMPO derivatives. We focused on calculated infrared (IR) vibrational stretching frequencies for the N=O bond in each oxoammonium T^+ species as these parameters have been an excellent platform for correlating structure to function in complex catalysis.[51,52]

The correlation between the calculated frequency of the N=O stretch ($v_{N=O}$) and the experimentally observed E_{a1} (Figure 5A) demonstrates that structures with a low E_{a1} also exhibit a relatively low $v_{N=O}$. This trend is corollary rather than causational. A lower E_{a1} oxidation potential is caused by stabilization of the oxoammonium cation of the T^+ species. This stabilization is a result of either geometric constraints or the presence of functional groups that can donate electron density to the empty p-orbital of the oxoammonium cation, which in turn gives the N=O bond more sp^3 character. Ultimately, this structural feature lowers $v_{N=O}$. Oxoammonium cation stabilization is exemplified in pairs of polycyclic structures that differ only by the presence of geminal methyl groups relative to the nitrogen atom (such as **13** vs **19**, **14** vs **20**, or **16** vs **22**, Figure 5C). In all cases, the structures with the geminal methyl group(s) exhibits a lower E_{a1} due to the stabilization of the resulting oxoammonium cation through hyperconjugation with the electron-donating methyl groups. In contrast to oxoammonium stabilization to lower E_{a1}, the opposite effect is observed in the presence of functional groups that destabilize the oxoammonium cation. Compounds that contain either a temporary or permanent cation (such as **7** or **28**, Figure 2) effectively increase the oxidation potential of the nitroxyl radical through coloumbic repulsion of cationic charges (as illustrated in Figure 5C). Similar effects have been observed for the oxidation potential of amine-containing ferrocene compounds and are highly dependent on the distance between the cationic moiety and the site of oxidation.[53]

Many of the same factors that affect the E_{a1} oxidation potential also affect the E_{a2} oxidation potential. As described earlier, E_{a2} is highly dependent on the protonation state of the TH species; so that E_{a2} increases under acidic conditions as the protonation equilibrium favors the TH_2^+ species and decreases under basic conditions where TH is favored. Therefore, many of the features that decrease E_{a1} through stabilization of the oxoammonium cation of T^+, will effectively increase E_{a2} through stabilization of the hydroxylammonium cation in TH_2^+.

A correlation exists between E_{a2} and the vibrational stretching frequency of the N−O* (v_{N-O*}) bond of the T^* state (as shown in Figure 5B), which is similar to that between
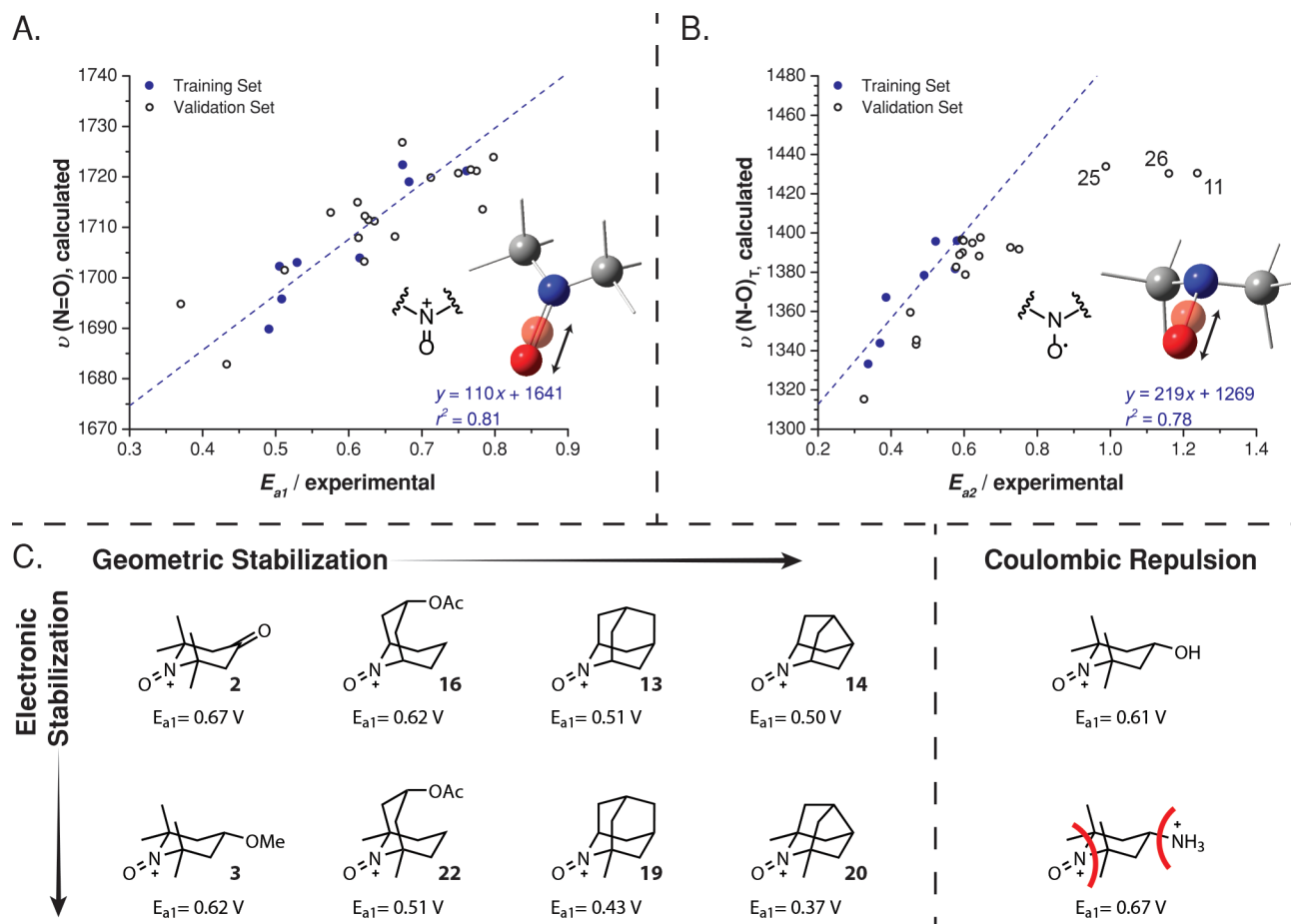
Figure 5. Correlation plots of computationally derived oxoammonium N═O (A) and nitroxyl radical N−O* (B) IR stretching frequencies versus E_{a1} and E_{a2} respectfully, and a chart indicating the effects of hybridization geometry of nitrogen, electronic character of the substituents and Coulombic repulsion on oxidation potential (C). In all cases, stabilization of the resulting ammonium cation results in a decreased oxidation potential. Structures are depicted to highlight the effect of geometric strain at N═O.

$v_{N═O}$ and E_{a1}. However, the v_{N-O*}/E_{a2} correlation arises from stabilization of the resulting radical species. Additionally, it should be noted that the correlation between E_{a2} and v_{N-O*} is weaker than that of E_{a1} and $v_{N═O}$. This is likely due to the additional dependence of E_{a2} on the protonation state of the **TH** species as described earlier.

Taken together, these two structure-function relationships demonstrate that the catalytic activity is increased through simultaneous destabilization of the oxoammonium cation, **T**$^+$, and the hydroxylammonium cation, **TH2**$^+$. However, it is important to note that destabilization of the off-cycle **TH$_2$**$^+$ species is significantly more important for increasing catalytic activity in aqueous systems because of the deactivating nature of the **TH$_2$**$^+$ formation. Therefore, the most effective strategy for enhancing catalytic activity of nitroxyl radicals involves the destabilization of **TH$_2$**$^+$ either by geometric constraints, hyperconjugative effects, or through Coulombic repulsion. Of particular note, these parameters are easily considered and used to anticipate the performance of proposed nitroxyl radical electrocatalyst.

Application of Nitroxyl Radical Compounds. As mentioned above, stable nitroxyl radical compounds can act as efficient and environmentally friendly catalysts for the oxidation of alcohols and amines; however, their use is not limited to synthetic applications. Exploiting the statistical mean of both the catalytic activity (described in terms of j_{max}) and E_{a1}

as demarcation lines, each of the compounds studied can be separated into one of four quadrants based on their electrochemical characteristics. A quadrant graph highlighting these categorizations is depicted in Figure 6. The purpose of this graph is to visualize the types of applications for which each of the nitroxyl radical structures might be suitable.

Both quadrants I and II contain nitroxyl radicals that exhibit high catalytic activity. However, quadrant I compounds display a lower E_{a1} and are potentially well-suited as anodic oxidation catalysts in the context of a fuel cell, while compounds in quadrant II may be more suited for electrosynthetic applications in which the oxidation potential is less important within the range described in Figure 6. Quadrant III compounds are easily oxidized but relatively unreactive as oxidation catalysts; these properties are desirable in the design and selection of effective antioxidants or radical traps.[47] Finally, quadrant IV derivatives are not easily oxidized and their oxidized form is relatively inactive. Therefore, these compounds are considered the most stable nitroxyl radical species and would be useful for applications in which an unreactive radical species is needed such as in vivo EPR imaging.[41] It should be noted that the most widely used oxidation catalyst and EPR label is TEMPO (**1**), likely due to ease of access. However, TEMPO is neither the best nitroxyl radical for either application.
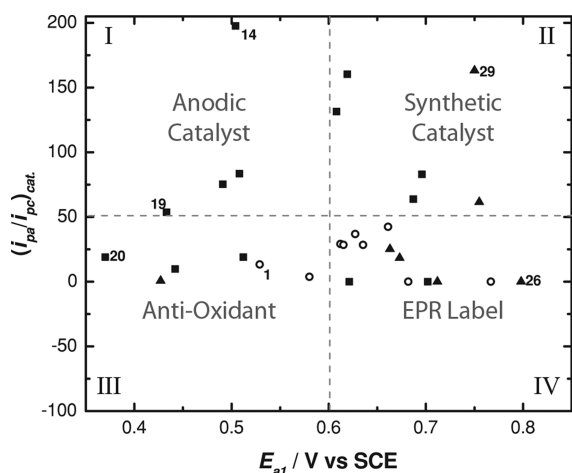
Figure 6. Plot of E_{a1} versus $(i_{pa}/i_{pc})_{cat}$ separated into four quadrants based on the corresponding statistical averages of all nitroxyl radical species studied. 4-Substituted TEMPO derivatives (O), 4N-substituted TEMPO derivatives (▲), and polycyclic species (■) are represented by different shapes. This is meant to aid in determining practical applications for any given species based on its relative electrochemical and catalytic characteristics.

CONCLUSION

We have reported a correlation between the difference in the oxidation potentials of nitroxyl radical-containing compounds and their activity as electrooxidation catalysts. Specifically, the catalytic activity is directly proportional to the inverse of the oxidation potentials, E_{a1} and E_{a2}, such that $(i_{pa}/i_{pc})_{cat} \sim 1/(E_{a2} - E_{a1})$. The value of E_{a1} was demonstrated to be directly dependent on the stability of the resulting oxoammonium cation, T^+, while the value of E_{a2} was shown to be reliant on the destabilization of the hydroxylammonium cation, TH_2^+, in the catalytic cycle.

The statistical analysis of a relatively large structural data set provides a convenient method for visualizing important characteristics of several water-soluble nitroxyl radical compounds. Using either the graph shown in Figure 6 or the corresponding data list (provided in the Supporting Information), it is easy to select a TEMPO derivative that is well-suited to a given application.

On the basis of the described correlation, DFT calculations were used to develop a model able to accurately predict the catalytic activity of several TEMPO derivatives. This model provides a computational basis for predicting the catalytic activity of nitroxyl radical catalysts in aqueous systems and thereby, allowing for a method of rational catalyst design without the need for synthesizing large libraries of TEMPO derivatives. Additional correlations between the computed N═O and N−O* IR stretching frequencies and E_{a1} and E_{a2}, respectively, provide further insights into the structure−function relationships from which the electrochemical potentials are derived. Ongoing studies are focused on expanding this model to nonaqueous systems and applying reported or newly designed nitroxyl radicals to various energy related goals.

ASSOCIATED CONTENT

S Supporting Information

The Supporting Information is available free of charge on the ACS Publications website at DOI: 10.1021/jacs.5b11252.

X-ray crystal data for selected synthetic intermediates. (CIF)

Materials, synthetic procedures, assignment of E_{a1} and E_{a2}, derivation of kinetic equations, pH dependence, computational methods, optimization of computational level of theory and basis set, sample CVs, spectra, summary of electrochemistry for each compound. (PDF)

AUTHOR INFORMATION

Corresponding Authors
*minteer@chem.utah.edu
*sigman@chem.utah.edu

Author Contributions
‖DPH and DAS contributed equally.

Notes
The authors declare no competing financial interest.

REFERENCES

(1) Neiman, M. B.; Rozantzev, E. G.; Mamedova, Y. G. *Nature* **1962**, *196*, 472−474.

(2) Golubev, V. A.; Rozantsev, É. G.; Neiman, M. B. *Bull. Acad. Sci. USSR, Div. Chem. Sci.* **1965**, *14*, 1898−1904.

(3) Ganem, B. *J. Org. Chem.* **1975**, *40*, 1998−2000.

(4) Keana, J. F. W. *Chem. Rev.* **1978**, *78*, 37−64.

(5) Kelen, T.; Tudos, F.; Balint, G.; Rockenbaur, A. In *Polymer Stabilization and Degradation*; American Chemical Society: Washington, D.C., 1985; Vol. *280*, pp 109−117.

(6) Villamena, F. A.; Zweier, J. L. *Antioxid. Redox Signaling* **2004**, *6*, 619−629.

(7) *Spin Labeling*; Berliner, L.; Reuben, J., Eds.; Springer: New York, 1989.

(8) Bobst, A. M.; Kao, S.-C.; Toppin, R. C.; Ireland, J. C.; Thomas, I. E. *J. Mol. Biol.* **1984**, *173*, 63−74.

(9) McConnell, H. M.; McFarland, B. G. *Q. Rev. Biophys.* **1970**, *3*, 91−136.

(10) Song, C.; Hu, K.-N.; Joo, C.-G.; Swager, T. M.; Griffin, R. G. *J. Am. Chem. Soc.* **2006**, *128*, 11385−11390.

(11) Krishna, M. C.; Grahame, D. A.; Samuni, A.; Mitchell, J. B.; Russo, A. *Proc. Natl. Acad. Sci. U. S. A.* **1992**, *89*, 5537−5541.

(12) Goldstein, S.; Merenyi, G.; Russo, A.; Samuni, A. *J. Am. Chem. Soc.* **2003**, *125*, 789−795.

(13) Goldstein, S.; Samuni, A.; Hideg, K.; Merenyi, G. *J. Phys. Chem. A* **2006**, *110*, 3679−3685.

(14) Rozantsev, E. G.; Sholle, V. D. *Synthesis* **1971**, *1971*, 401−414.

(15) Bobbitt, J. M.; Flores, C. L. *Heterocycles* **1988**, *27*, 509−533.

(16) Ma, Z.; Bobbitt, J. M. *J. Org. Chem.* **1991**, *56*, 6110−6114.

(17) Rychnovsky, S. D.; McLernon, T. L.; Rajapakse, H. *J. Org. Chem.* **1996**, *61*, 1194−1195.

(18) Schnatbaum, K.; Schäfer, H. J. *Synthesis* **1999**, *1999*, 864−872.

(19) Fabbrini, M.; Galli, C.; Gentili, P.; Macchitella, D. *Tetrahedron Lett.* **2001**, *42*, 7551−7553.

(20) Hoover, J. M.; Stahl, S. S. *J. Am. Chem. Soc.* **2011**, *133*, 16901−16910.

(21) Lauber, M. B.; Stahl, S. S. *ACS Catal.* **2013**, *3*, 2612−2616.

(22) Ryland, B. L.; Stahl, S. S. *Angew. Chem., Int. Ed.* **2014**, *53*, 8824−8838.

(23) Zhao, M.; Li, J.; Mano, E.; Song, Z.; Tschaen, D. M.; Grabowski, E. J. J.; Reider, P. J. *J. Org. Chem.* **1999**, *64*, 2564−2566.

(24) Steelink, C.; Britton, W. E. *Tetrahedron Lett.* **1974**, *15*, 2869−2872.

(25) Semmelhack, M. F.; Chou, C. S.; Cortes, D. A. *J. Am. Chem. Soc.* **1983**, *105*, 4492−4494.

(26) Miyazawa, T.; Endo, T.; Shiihashi, S.; Okawara, M. *J. Org. Chem.* **1985**, *50*, 1332−1334.

(27) Miyazawa, T.; Endo, T. *J. Org. Chem.* **1985**, *50*, 3930−3931.

(28) Semmelhack, M. F.; Schmid, C. R. *J. Am. Chem. Soc.* **1983**, *105*, 6732−6734.

(29) Semmelhack, M. F.; Schmid, C. R.; Cortés, D. A. *Tetrahedron Lett.* **1986**, *27*, 1119−1122.

(30) Bailey, W. F.; Bobbitt, J. M.; Wiberg, K. B. *J. Org. Chem.* **2007**, *72*, 4504−4509.

(31) Comminges, C.; Barhdadi, R.; Doherty, A. P.; O'Toole, S.; Troupel, M. *J. Phys. Chem. A* **2008**, *112*, 7848−7855.

(32) Bobbitt, J. M. *ChemInform* **2011**, *42*, no.

(33) Rychnovsky, S. D.; Beauchamp, T.; Vaidyanathan, R.; Kwan, T. *J. Org. Chem.* **1998**, *63*, 6363−6374.

(34) Shibuya, M.; Pichierri, F.; Tomizawa, M.; Nagasawa, S.; Suzuki, I.; Iwabuchi, Y. *Tetrahedron Lett.* **2012**, *53*, 2070−2073.

(35) Doi, R.; Shibuya, M.; Murayama, T.; Yamamoto, Y.; Iwabuchi, Y. *J. Org. Chem.* **2015**, *80*, 401−413.

(36) Shibuya, M.; Tomizawa, M.; Suzuki, I.; Iwabuchi, Y. *J. Am. Chem. Soc.* **2006**, *128*, 8412−8413.

(37) Manda, S.; Nakanishi, I.; Ohkubo, K.; Yakumaru, H.; Matsumoto, K.-i.; Ozawa, T.; Ikota, N.; Fukuzumi, S.; Anzai, K. *Org. Biomol. Chem.* **2007**, *5*, 3951−3955.

(38) Rafiee, M.; Miles, K. C.; Stahl, S. S. *J. Am. Chem. Soc.* **2015**, *137*, 14751.

(39) Hickey, D. P.; McCammant, M. S.; Giroud, F.; Sigman, M. S.; Minteer, S. D. *J. Am. Chem. Soc.* **2014**, *136*, 15917−15920.

(40) Nigam, S.; Asmus, K.-D.; Willson, R. L. *J. Chem. Soc., Faraday Trans. 1* **1976**, *72*, 2324−2340.

(41) Fish, J. R.; Swarts, S. G.; Sevilla, M. D.; Malinski, T. *J. Phys. Chem.* **1988**, *92*, 3745−3751.

(42) Kato, Y.; Shimizu, Y.; Yijing, L.; Unoura, K.; Utsumi, H.; Ogata, T. *Electrochim. Acta* **1995**, *40*, 2799−2802.

(43) Ma, Y.; Loyns, C.; Price, P.; Chechik, V. *Org. Biomol. Chem.* **2011**, *9*, 5573−5578.

(44) Jorgensen, W. L.; Chandrasekhar, J.; Madura, J. D.; Impey, R. W.; Klein, M. L. *J. Chem. Phys.* **1983**, *79*, 926−935.

(45) Rychnovsky, S. D.; Vaidyanathan, R.; Beauchamp, T.; Lin, R.; Farmer, P. J. *J. Org. Chem.* **1999**, *64*, 6745−6749.

(46) Hodgson, J. L.; Roskop, L. B.; Gordon, M. S.; Lin, C. Y.; Coote, M. L. *J. Phys. Chem. A* **2010**, *114*, 10458−10466.

(47) Hodgson, J. L.; Namazian, M.; Bottle, S. E.; Coote, M. L. *J. Phys. Chem. A* **2007**, *111*, 13595−13605.

(48) Frisch, M. J.; Trucks, G. W.; Schlegel, H. B.; Scuseria, G. E.; Robb, M. A.; Cheeseman, J. R.; Scalmani, G.; Barone, V.; Mennucci, B.; Petersson, G. A.; Nakatsuji, H.; Caricato, M.; Li, X.; Hratchian, H. P.; Izmaylov, A. F.; Bloino, J.; Zheng, G.; Sonnenberg, J. L.; Hada, M.; Ehara, M.; Toyota, K.; Fukuda, R.; Hasegawa, J.; Ishida, M.; Nakajima, T.; Honda, Y.; Kitao, O.; Nakai, H.; Vreven, T.; Montgomery Jr., J. A.; Peralta, J. E.; Ogliaro, F. o.; Bearpark, M. J.; Heyd, J.; Brothers, E. N.; Kudin, K. N.; Staroverov, V. N.; Kobayashi, R.; Normand, J.; Raghavachari, K.; Rendell, A. P.; Burant, J. C.; Iyengar, S. S.; Tomasi, J.; Cossi, M.; Rega, N.; Millam, N. J.; Klene, M.; Knox, J. E.; Cross, J. B.; Bakken, V.; Adamo, C.; Jaramillo, J.; Gomperts, R.; Stratmann, R. E.; Yazyev, O.; Austin, A. J.; Cammi, R.; Pomelli, C.; Ochterski, J. W.; Martin, R. L.; Morokuma, K.; Zakrzewski, V. G.; Voth, G. A.; Salvador, P.; Dannenberg, J. J.; Dapprich, S.; Daniels, A. D.; Farkas, Ã.-d. n.; Foresman, J. B.; Ortiz, J. V.; Cioslowski, J.; Fox, D. J. *Gaussian 09*; Gaussian, Inc.: Wallingford, CT, 2009.

(49) Fu, Y.; Liu, L.; Yu, H.-Z.; Wang, Y.-M.; Guo, Q.-X. *J. Am. Chem. Soc.* **2005**, *127*, 7227−7234.

(50) Tripkovic, V.; Björketun, M. E.; Skúlason, E.; Rossmeisl. *Phys. Rev. B: Condens. Matter Mater. Phys.* **2011**, *84*, 115452.

(51) Milo, A.; Bess, E. N.; Sigman, M. S. *Nature* **2014**, *507*, 210−214.

(52) Milo, A.; Neel, A. J.; Toste, F. D.; Sigman, M. S. *Science* **2015**, *347*, 737−743.

(53) Benito, A.; Martinez-Manez, R.; Soto, J.; Tendero, M. J. L. *J. Chem. Soc., Faraday Trans.* **1997**, *93*, 2175−2180.